

Enhanced coherent phonon excitation in Fe₃GeTe₂ via resonance Raman effectJia Guo,^{1,*} Chenhui Zhang^{1,2,*}, Weizheng Liang^{1,†}, Xi-Xiang Zhang^{1,2} and S. N. Luo^{3,‡}¹*The Peac Institute of Multiscale Sciences, Chengdu, Sichuan, People's Republic of China*²*Physical Science and Engineering Division, King Abdullah University of Science and Technology, Thuwal 23955-6900, Saudi Arabia*³*School of Materials Science and Engineering, Southwest Jiaotong University, Chengdu, Sichuan, People's Republic of China*

(Received 18 September 2020; revised 27 October 2020; accepted 7 January 2021; published 21 January 2021)

Coherent phonon excitation via femtosecond laser pulses can be used to control physical properties of matter, and enhancing coherent phonon excitation is highly relevant. Here, we report the strong enhancement of coherent phonon excitation in Fe₃GeTe₂ (FGT) via the resonance Raman effect. On the basis of the femtosecond transient optical spectroscopy measurements, the A_{1g} coherent phonon excitation in FGT is obtained as a function of pump photon energy. Its excitation can be maximized by tuning the pump photon energy. The maximum coherent phonon excitation at the 1.574-eV pump photon energy corresponds to an electronic transition in FGT, and is a direct result of the resonance Raman effect. The A_{1g} coherent phonon generation follows the impulsive stimulated Raman scattering mechanism. Our work demonstrates that the resonance Raman effect can be an effective way to enhance coherent phonon excitation via electronic excitation.

DOI: [10.1103/PhysRevB.103.024302](https://doi.org/10.1103/PhysRevB.103.024302)**I. INTRODUCTION**

Coherent phonons can be exploited for collective coherent control over the transient states of matter via driving periodic lattice vibrations. Inducing superconductivity in cuprates [1–3], triggering polarization in ferroelectrics and quantum paraelectrics [4,5], controlling the topological band structures of topological materials [6,7], and engineering electronic transport of complex oxides [8], all via coherent phonons, have been demonstrated. To control the physical properties of matter, a strong excitation of coherent phonons is necessary, and how to enhance coherent phonon excitation has been of interest.

Direct coupling of light to infrared-active vibration and ionic Raman scattering have been demonstrated as effective ways to induce strong coherent phonon excitation [1,9,10]. However, coupling light to infrared-active vibration requires an electric dipole in materials, which limits its application. Ionic Raman scattering pumps a material using a THz pulse with a fixed frequency close to the phonon frequency, and can increase coherent phonon excitation by increasing the strength of incident THz pulses [9]. It has been demonstrated to drive strong periodic lattice vibrations in solids and used to manipulate materials' properties [1,9]. However, the access to intense THz radiation is still difficult. Nonequilibrium hot carrier decay via electron-phonon coupling can also excite coherent phonons [11–14]; the excited nonequilibrium hot carrier releases their excess energy to lattice via exciting coherent phonons (Fig. 1). However, how to enlarge coherent phonon excitation via electron-phonon coupling remains unexplored.

Here, we report strong enhancement of coherent phonon excitation in Fe₃GeTe₂ (FGT) by tuning pump photon energy, measured with femtosecond transient optical spectroscopy (FTOS). The FGT single crystal is an itinerant van der Waals ferromagnet with a ferromagnet-paramagnet transition near 150–230 K [15–22]. The FTOS measurements are conducted in a pump photon energy range of 1.544–1.656 eV, and a temperature range of 5–350 K, at different pump fluences. We observe the strong dependence of coherent phonon excitation on pump photon energy. The maximum coherent phonon excitation occurs at the 1.574-eV pump photon energy, corresponding to the energy of an electronic transition in FGT and a result of the resonance Raman effect. Our experiments demonstrate the potential of manipulating physical properties with strong coherent phonon excitation via the resonance Raman effect.

II. EXPERIMENT

FGT single crystals are grown by the chemical vapor transport method. Powders of high-purity Fe (99.99%), Ge (99.99%), and Te (99.99%) are mixed at a stoichiometric ratio of 3:1:2 and pressed into a pellet and then placed into a quartz tube. The sealed quartz tube is set in an oven with a temperature gradient from 1023 K to 973 K for a week. The FGT pellet is placed at the hot end of the quartz tube and vaporizes gradually, and single-crystal FGT grows at the cold end via vapor deposition. Before being loaded on a cooling stage for the FTOS experiments, an FGT single crystal is cleaved with scotch tape to obtain a fresh surface. The schematic setup for FTOS was presented elsewhere [23]. We use a Ti:sapphire laser with a 80-MHz repetition rate and a 35-fs pulse duration for the FTOS measurements. The central wavelength of the Ti:sapphire laser can be tuned between 749 nm and 803 nm (photon energy 1.656–1.544 eV). The pump laser fluence is tuned in the range of 5.4–90 μJ/cm²,

*These authors contributed equally to this work.

†wzliang@pims.ac.cn

‡sluo@swjtu.edu.cn

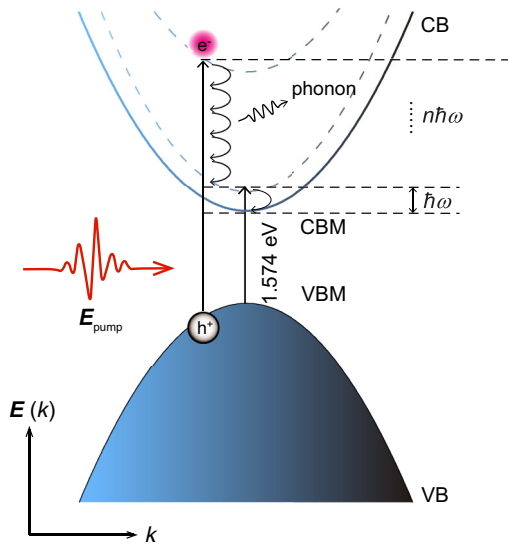


FIG. 1. Diagram of the coherent phonon excitation. CB: conduction band; VB: valence band; CBM: conduction band minimum; VBM: valence band maximum; e^- : electron; h^- : hole; E : energy; k : wave vector.

while the probe laser fluence is fixed at $0.5 \mu\text{J}/\text{cm}^2$. Both degenerate and nondegenerate pump-probe measurements are conducted. For degenerate pump-probe measurements, the pump and probe laser frequencies are the same. For nondegenerate pump-probe measurements, we use a second harmonic generation crystal barium diboron tetra oxide (BBO) to double the frequency, and a bandpass filter ($400 \pm 20 \text{ nm}$) to filter out the residual near-infrared component, and the energy-doubled laser beam is used for pump. A discussion refers to degenerate measurements unless stated otherwise. A Montana cryostation system is used for temperature control.

III. RESULTS

Figure 2 shows color maps of $\Delta R(t)/R_0$ time series at different temperatures (T) for single-crystal FGT collected at various pump photon energies in degenerate pump-probe

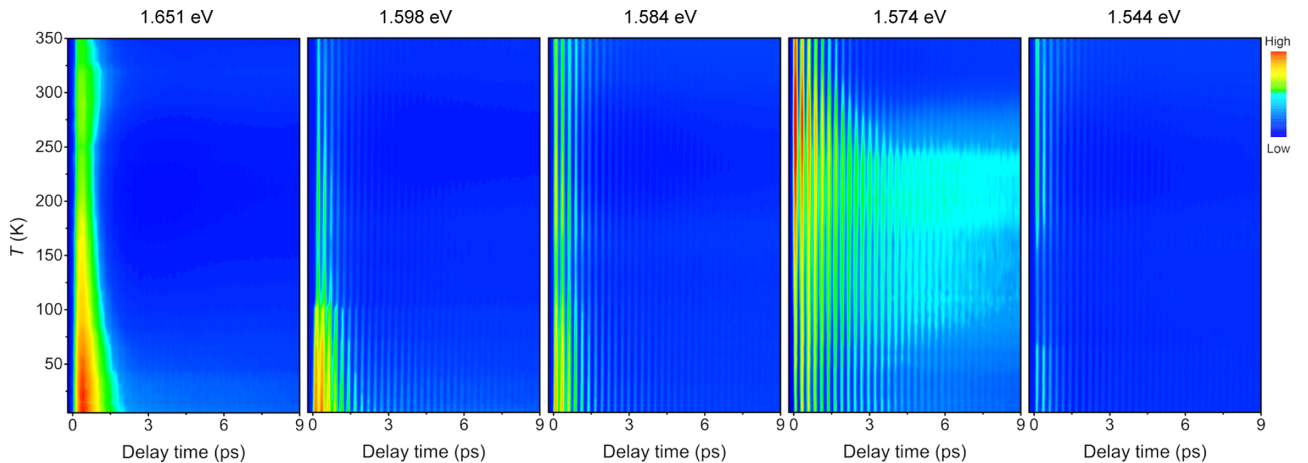


FIG. 2. Color maps of $\Delta R(t)/R_0$ time series at different temperatures (T) for single crystal FGT collected with different pump photon energies. Pump fluence: $10 \mu\text{J}/\text{cm}^2$, and probe fluence: $0.5 \mu\text{J}/\text{cm}^2$.

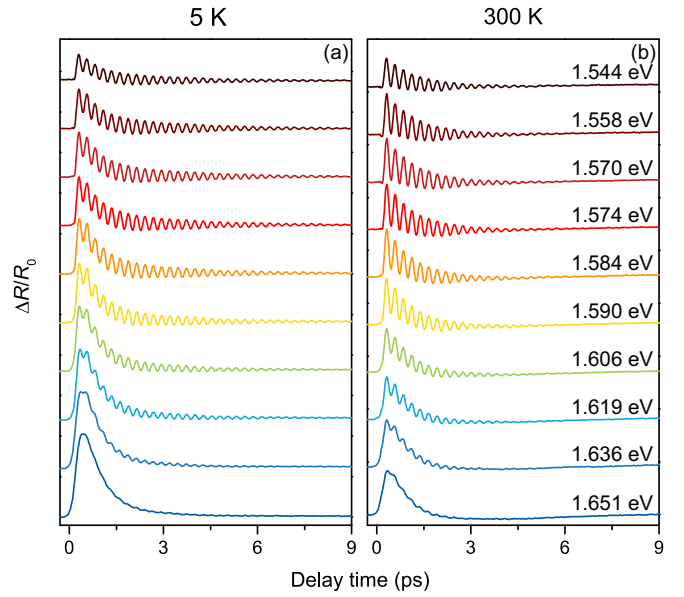


FIG. 3. $\Delta R(t)/R_0$ time series collected with different pump photon energies at (a) 5 K and (b) 300 K. Pump fluence: $10 \mu\text{J}/\text{cm}^2$; probe fluence: $0.5 \mu\text{J}/\text{cm}^2$.

measurements. Here $\Delta R = R - R_0$ is differential reflectivity, R denotes current total reflectivity, and R_0 refers to the total reflectivity without pump. Immediately after the femtosecond laser pump, $\Delta R/R_0$ exhibits an instantaneous rise at time $t = 0 \text{ ps}$, as a result of photoexcitation of hot carriers from the valence band to the conduction band. The most pronounced difference among the $\Delta R(t)/R_0$ time series collected at various pump photon energies lies in the damping oscillations as seen in the color maps, which are due to the reflectivity modulation by coherent phonons in FGT. The oscillation signal is the strongest when the pump photon energy is 1.574 eV, indicating the strong pump photon energy dependence of the coherent phonon excitation in FGT. Figure 3 shows more detailed $\Delta R(t)/R_0$ time series collected with various pump photon energies at 5 K and 300 K. The intensity of the

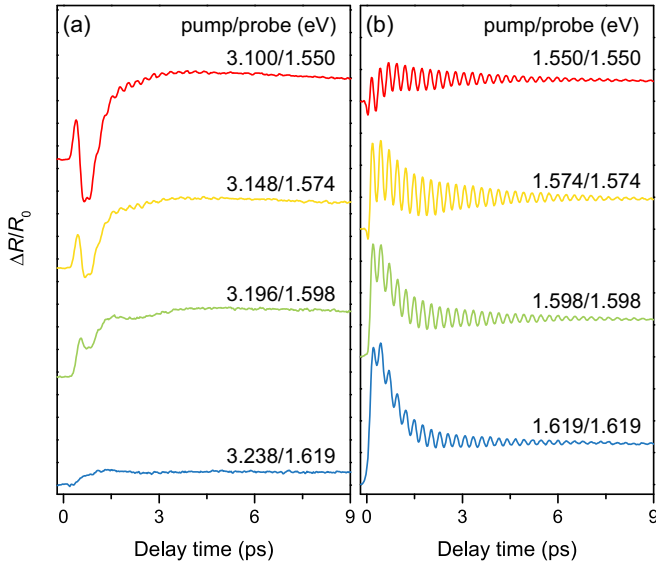


FIG. 4. (a) Nondegenerate and (b) degenerate pump-probe measurements on $\Delta R(t)/R_0$ time series at different pump photon energies. Pump fluence: $10 \mu\text{J}/\text{cm}^2$; probe fluence: $0.5 \mu\text{J}/\text{cm}^2$.

oscillation signal is strongly dependent on the pump photon energy at both temperatures.

$\Delta R(t)/R_0$ time series are also measured in the nondegenerate mode, and compared to their counterparts in the degenerate mode (Fig. 4). In the degenerate and corresponding nondegenerate pump-probe measurements, the probe measures the same electronic band level of FGT with the same photon frequency, while electrons are excited to different electronic band levels due to different pump photon energies. The $\Delta R(t)/R_0$ time series from the degenerate pump-probe measurements show strong coherent phonon oscillations, but such oscillations are much weaker or negligible in the nondegenerate pump-probe measurements due to the considerably higher pump photon energy.

The coherent phonon vibrations can be measured by FTOS as the periodic oscillations in the $\Delta R(t)/R_0$ time series. To the first-order approximation, the reflectivity modulation induced by coherent phonons can be expressed as [24,25]

$$\Delta R(t)/R_{0op} = \frac{\partial[\Delta R(t)/R_0]}{\partial Q} Q = \frac{\partial[\Delta R(t)/R_0]}{\partial Q} A_{op} Q_0, \quad (1)$$

where Q is the coordinates of coherent phonon and $Q_0 = \exp[-(t - t_0)/\tau_{op}] \cos(\omega t + \phi)$ is the normalized coordinates of coherent phonon. A_{op} , τ_{op} , ω , and ϕ are amplitude, dephasing time, angular frequency, and the initial phase of the damping oscillations of coherent optical phonons, respectively. The subscript op denotes the optical phonon. More excited phonons will induce larger oscillations in $\Delta R/R_0$.

The $\Delta R(t)/R_0$ time series can be described with the combination of exponential functions and a damping oscillation function, i.e.,

$$\Delta R(t)/R_0 = A_{ep} \exp\left(-\frac{t - t_0}{\tau_{ep}}\right) + A_{op} \exp\left(-\frac{t - t_0}{\tau_{op}}\right) \cos(\omega t + \phi) + C. \quad (2)$$

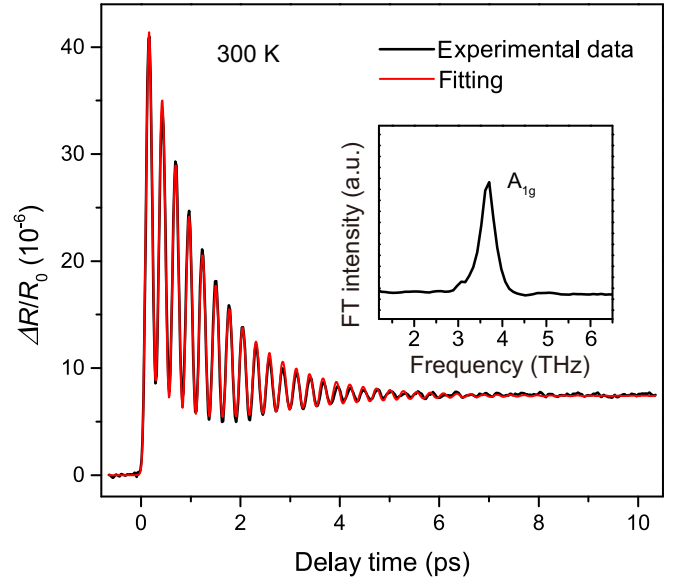


FIG. 5. $\Delta R(t)/R_0$ time series collected at 300 K with a pump energy of 1.574 eV, along with the fitting with the combination of an exponential function and a damping oscillation function. The inset is the fast Fourier transform (FFT) of the oscillation components, revealing the A_{1g} -mode coherent phonon of FGT. Pump fluence: $10 \mu\text{J}/\text{cm}^2$; probe fluence: $0.5 \mu\text{J}/\text{cm}^2$.

Here A_{ep} and τ_{ep} are the amplitude and decay time of the nonoscillation component, representing the hot carrier decay due to the electron-phonon coupling. (The subscript ep denotes electron-phonon coupling.) The second term represents the damping oscillation component due to coherent phonon oscillation and decay. C is a fitting constant.

We use the $\Delta R(t)/R_0$ time series at 300 K with the 1.574-eV laser pump as an example of fitting with the above equation (Fig. 5). The fitting yields $A_{op} = (10.68 \pm 0.02) \times 10^{-6}$, $\tau_{op} = 1.36 \pm 0.01$ ps, $\omega = (23.93 \pm 0.02) \times 10^{12}$ rad/s, and $\phi = 3.03 \pm 0.06 \approx \pi$ rad, referred to as the coherent phonon dynamics parameters. The frequency of the oscillation component is $\omega/2\pi \approx 3.81$ THz (126.8 cm^{-1}), suggesting that the coherent phonon is of the A_{1g} mode [26,27]. The fitting also yields $A_{ep} = (8.71 \pm 0.02) \times 10^{-6}$, and $\tau_{ep} = 0.88 \pm 0.01$ ps for the nonoscillation component, which are referred to as the hot carrier dynamics parameters.

Figure 6 shows the color map of the $\Delta R(t)/R_0$ time series at different pump laser polarizations. The $\Delta R(t)/R_0$ time series, including the coherent phonon oscillation component, remains unchanged upon varying pump polarization, i.e., the coherent phonon oscillation is independent of pump laser polarization, consistent with the full symmetry of the A_{1g} mode.

Given the $\Delta R(t)/R_0$ time series, we can obtain A_{op} at different pump photon energies. Figure 7 show the A_{op} of the A_{1g} coherent phonon as a function of pump photon energy at 5 K and 300 K. The pump fluence is fixed at $10 \mu\text{J}/\text{cm}^2$, and the probe laser fluence, at $0.5 \mu\text{J}/\text{cm}^2$. Corrections are made to consider the wavelength-dependence of the reflectivity. The maximum A_{op} appears at the 1.574-eV pump photon energy for both temperatures, and increasing or reducing pump photon energy results in decreased A_{op} . The A_{op} values at 300 K are lower than those at 5 K.

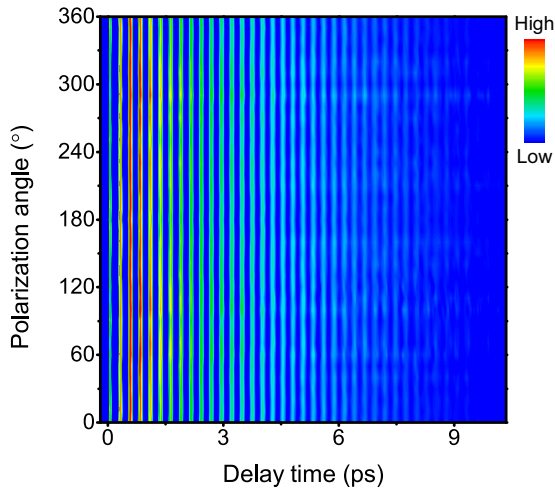


FIG. 6. Color map of $\Delta R(t)/R_0$ time series at different pump polarization angles with the 1.574-eV laser pump at 5 K. Pump fluence: $10 \mu\text{J}/\text{cm}^2$; probe fluence: $0.5 \mu\text{J}/\text{cm}^2$.

We also explore the effect of pump fluence on coherent phonon oscillations. Figure 8 shows the $\Delta R(t)/R_0$ time series collected at 5 K with three representative pump photon energies, 1.619 eV, 1.574 eV, and 1.544 eV, for pump fluences ranging from $5.4 \mu\text{J}/\text{cm}^2$ to $90 \mu\text{J}/\text{cm}^2$. Such measurements are conducted in the pump photon energy range of 1.544–1.656 eV. The intensity of $\Delta R(t)/R_0$, as well as the coherent phonon oscillation component, increases with increasing pump fluence (F).

We fit the $\Delta R(t)/R_0$ time series at different pump fluences with Eq. (2), and obtain A_{op} as a function of pump fluence for different pump photon energies [Fig. 9(a)]. All the $A_{\text{op}}(F)$ curves obtained at different pump photon energies are linear with a positive slope, but different in the slope values. To quantify the coherent phonon excitation efficiency in terms of pump photon energy, we define the photosusceptibility of the A_{1g} coherent phonon at a given pump photon energy as $\chi = dA_{\text{op}}/dF$. χ is obtained as a function of pump

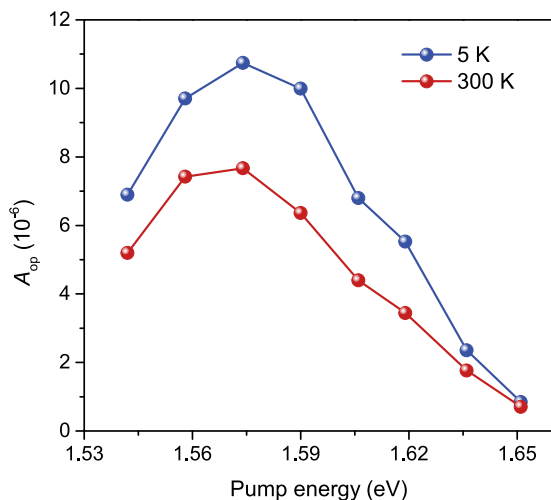


FIG. 7. A_{op} as a function of pump photon energy at 5 K and 300 K. Pump fluence: $10 \mu\text{J}/\text{cm}^2$; probe fluence: $0.5 \mu\text{J}/\text{cm}^2$.

photon energy from linear fittings in Fig. 9(a), and plotted in Fig. 9(b). χ increases and then decreases rapidly with increasing pump photon energy, with the maximum $\chi = 9.9262 \times 10^{-7} \mu\text{J}^{-1}\text{cm}^2$ at 1.574 eV. For example, a slight increase of pump photon energy from 1.574 eV to 1.651 eV induces a reduction in χ by a factor of ~ 15 .

IV. DISCUSSION

FGT undergoes the ferromagnetic-paramagnetic transition near about 220 K. The spin-ordering in magnetic materials can influence coherent phonon excitation [28]. However, the A_{1g} coherent phonon excitation shows a strong pump photon energy dependence at both 5 K and 300 K (Figs. 3 and 7), indicating that the A_{1g} coherent phonon excitation is not correlated to the ferromagnetic-paramagnetic transition in FGT. For coherent phonon excitation via electron-phonon coupling in a hot carrier decay process, an electron in a low energy state is excited into a high-energy state by femtosecond laser pump, and then the excited electron returns to the initial state by releasing their excess energy via exciting bosons [29]; the excited bosons are coherent phonons, and each phonon take an energy of $\hbar\omega$ (angular frequency ω) from the hot carrier. One would expect more coherent phonons excited with a higher pump photon energy (Fig. 1). However, the strongest coherent phonon excitation occurs at a specific pump photon energy (1.574 eV) across a pump photon energy range of 1.544–1.651 eV. Therefore, there should exist an electronic transition in FGT with an energy gap of ~ 1.574 eV, and electron hopping in this electron transition strengthens the A_{1g} mode coherent phonon excitation. As shown by the first-principles calculation [30], there are two electronic transitions with gaps close to 1.574 eV: one from an Fe d orbital state below the Fermi level E_F to an Fe d orbital state above E_F , and the other from an Fe d orbital state below E_F to a Te p orbital state above E_F . Since the gaps of these two electronic transitions are too close, the exact transition cannot be identified with FTOS.

The strong enhancement of the A_{1g} phonon excitation at the 1.574-eV pump photon energy in FGT in our FTOS measurements points to the resonance Raman effect. The resonance Raman effect is a Raman scattering enhancement phenomenon via tuning the pump photon energy to the energy of an electronic transition, and can enhance the Raman scattering intensity by a factor of 10^2 – 10^6 [31]. The enhancement of coherent phonon excitation via the resonance Raman effect was also investigated by calculation [32] and experiments [33–35]. However, the phonon excitation mechanism and the effects of the enhanced coherent phonon excitation on the hot carrier and phonon decay were unclear.

The resonance Raman effect involves an electronic transition between a low energy level and a high energy level, and their gap is ΔE . To induce a Raman resonance effect, the pump photon energy must be tuned to satisfy that $E = \Delta E + \hbar\omega$. Here, $\hbar\omega$ represents the energy of an excited phonon. For a phonon with $\omega/2\pi = 3.81$ THz, $\hbar\omega = 0.01538$ eV. In our experiment, the maximum coherent phonon excitation via the resonance Raman effect is obtained at a 1.574-eV laser pump in FGT. Hence, the energy gap of the electronic transition in FGT is $\Delta E = 1.559$ eV.

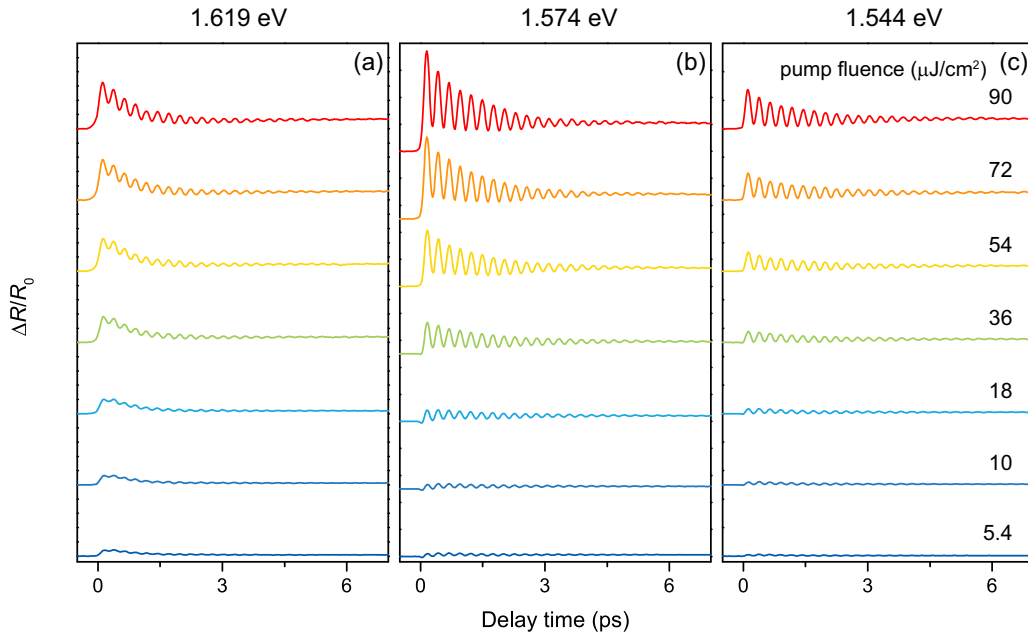


FIG. 8. $\Delta R(t)/R_0$ collected at 5 K with pump photon energies of (a) 1.619 eV, (b) 1.574 eV, and (c) 1.544 eV, and different pump fluences as noted. Probe fluence: $0.5 \mu\text{J}/\text{cm}^2$.

We now discuss the mechanism for coherent phonon generation. The ionic Raman scattering mechanism is unlikely since it requires that pump photon energy be close to coherent phonon energy (in the 1–100 meV range), and the pump photon energy in our experiments is much higher (1.544–1.656 eV) [9]. In general, the excitation of coherent optical phonons via femtosecond laser with a wavelength in the near infrared region is believed to be initiated either via impulsive stimulated Raman scattering (ISRS) [13,14], or dispersive excitation of coherent phonons (DECP) [11,12].

In the DECP mechanism, instantaneous redistribution of the nonequilibrium carriers via laser pump is the driving force of phonon excitation and the coherent phonon excitation depends on density of laser-excited nonequilibrium carriers n_s [36]. In our measurements, only the A_{1g} coherent phonon is excited (Fig. 5, inset), and A_{op} is linearly dependent on pump fluence in a pump photon energy range of 1.544–1.651 eV [Fig. 9(a)].

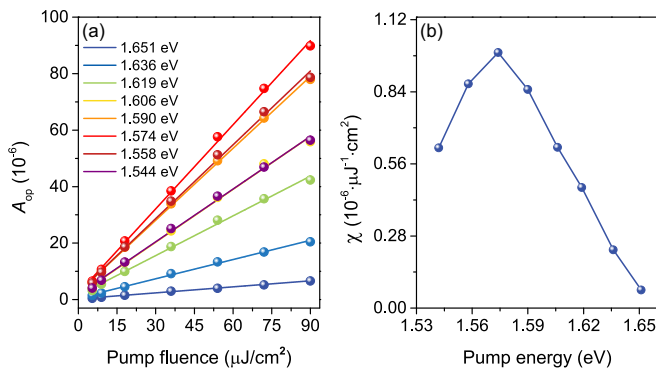


FIG. 9. (a) A_{op} as a function of pump fluence at 5 K with different pump photon energies as noted. (b) Photosusceptibility of the A_{1g} coherent phonon as a function of pump photon energy at 5 K.

The fitting to the $\Delta R(t)/R_0$ time series collected at 300 K with a pump fluence of $10 \mu\text{J}/\text{cm}^2$ yields $A_{ep} = (8.71 \pm 0.02) \times 10^{-6}$ and $A_{op} = (10.68 \pm 0.02) \times 10^{-6}$ at 1.574 eV, while $A_{ep} = (8.03 \pm 0.02) \times 10^{-6}$ and $A_{op} = (0.71 \pm 0.02) \times 10^{-6}$ at 1.651 eV. The A_{ep} values are close, indicating that a slight increase of pump photon energy from 1.574 eV to 1.651 eV results in a negligible change in n_s . On the other hand, A_{op} obtained at 1.574 eV is significantly higher (by a factor of ~ 15) than that at 1.651 eV. If DECP were the mechanism for the A_{1g} coherent phonon excitation in FGT, the A_{op} values would be similar for the 1.574-eV and 1.651-eV pump photon energies, in contrast to the experimental observation. Therefore, DECP is an unlikely mechanism for the A_{1g} coherent phonon excitation in FGT, and the only likely mechanism is ISRS.

For the ISRS mechanism under the two-band condition, the coherent phonon excitation is enhanced considerably when the pump photon energy is close to the energy of the electronic transition between these two transition bands [13,33–35,37]. Indeed, the pump photon energy dependence of the A_{1g} coherent phonon excitation in the FGT (Fig. 9) points to the resonant ISRS mechanism under the two-band condition.

The strong A_{1g} coherent phonon excitation via the resonance Raman effect may induce distortion in FGT, thus modifying the dynamics of hot carrier and coherent phonon decays. We first discuss the effect of the enhancement of coherent phonon excitation on the hot carrier decay. Figure 10(a) shows the temperature dependence of τ_{ep} in FGT collected at various pump photon energies. τ_{ep} represents the hot carrier decay time via electron-phonon coupling. All the τ_{ep} values obtained at different pump photon energies show similar temperature dependence, except for the 1.574-eV pump photon energy.

The anomalous temperature dependence of τ_{ep} obtained at the 1.574-eV pump photon energy is a result of the

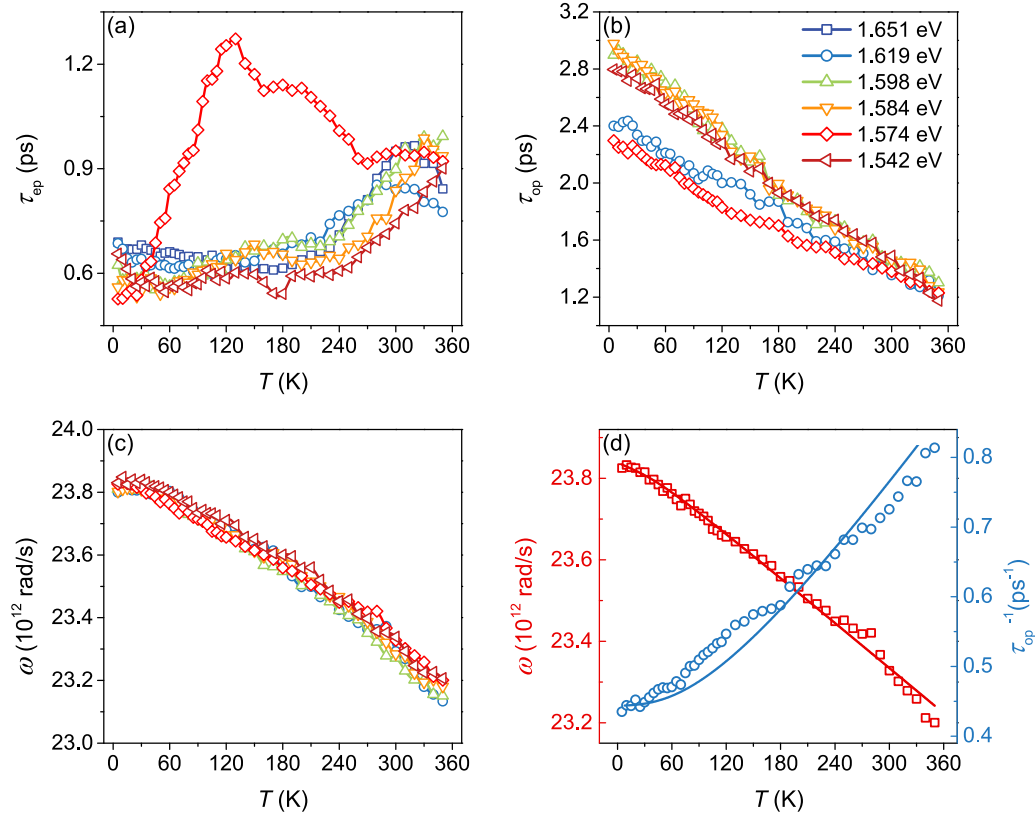


FIG. 10. (a)–(c) Temperature dependencies of τ_{ep} , τ_{op} and ω of FGT collected at various pump photon energies. (d) Temperature dependencies of ω and dephasing rate (τ_{op}^{-1}) collected at the 1.574-eV laser pump. Symbols: measurements; red line: fitting with Eq. (5); blue line: fitting with Eq. (6). Pump fluence: $10 \mu\text{J}/\text{cm}^2$; probe fluence: $0.5 \mu\text{J}/\text{cm}^2$.

enhancement of coherent phonon excitation via the resonance Raman effect. The enhancement of coherent phonon excitation normally strengthens electron-phonon coupling. Under a fixed pump fluence, the strength of electron-phonon coupling $\lambda\langle\omega^2\rangle \propto \tau_{ep}^{-1}$ [38]. The stronger electron-phonon coupling induces a smaller τ_{ep} , i.e., a quicker hot carrier decay [39–41]. However, τ_{ep} is the longest in most of the temperature range for the 1.574-eV pump photon energy, suggesting weakened electron-phonon coupling, in contrast with certain previous reports [39–41]. The contradiction in electron-phonon coupling may due to the pronounced coherent phonon excitation via the resonance Raman effect, which re-excites the hot carrier, as observed in narrow-band materials. This is the so-called “bottleneck effect” [36,42], which occurs when an energy gap opens as a result of the competition between phonon emission during the decay of quasiparticles and the generation of quasiparticles by phonons. However in FGT, an energy gap is not open up, and its pronounced coherent phonon excitation may re-excites the hot carrier, giving rise to a longer τ_{ep} .

We discuss next phonon anharmonicity in FGT experiencing the resonance Raman effect. The τ_{op} values obtained at the 1.574-eV pump photon energy are also the smallest among all the pump photon energies explored, in particular, at low temperatures [Fig. 10(b)]. However, the $\omega(T)$ curves at different pump photon energies overlap with each other [Fig. 10(c)]; the insensitivity of $\omega(T)$ to the pump photon energy indicates the negligible thermal effect induced

by the pump laser, even for the 1.574-eV pump photon energy.

Both lattice thermal expansion and anharmonic phonon-phonon interaction contribute to the red shift in frequency of coherent optical phonons with increasing temperature [43]. The temperature-dependent optical phonon frequency can be written as [44,45]

$$\omega(T) = \omega_0 + \Delta\omega^{(1)}(T) + \Delta\omega^{(2)}(T), \quad (3)$$

where ω_0 is the intrinsic phonon frequency at 0 K, $\Delta\omega^{(1)}$ is the frequency shift due to lattice thermal expansion and $\Delta\omega^{(2)}$ is due to anharmonic phonon-phonon interaction. The contribution of thermal expansion is [44,45]

$$\Delta\omega^{(1)}(T) = \omega_0 \left[\exp \left(-\gamma \int_0^T (\alpha_a + \alpha_b + \alpha_c) dT' \right) - 1 \right]. \quad (4)$$

Here γ is the mode Grüneisen parameter, and α_a , α_b , and α_c are linear thermal expansion coefficients along the a -, b -, and c -axes, respectively. Since the values for these parameters are not available, the estimated values are used: $\gamma \sim 1-2$, and α_a , α_b , and α_c are $\sim 10^{-6} \text{K}^{-1}$.

In anharmonic phonon-phonon interaction, the three-phonon process is the most common way for optical phonon decay, in which an optical phonon (ω_0) decays into two acoustic phonons with identical frequencies but opposite wave vectors ($\omega_1 = \omega_2 = \omega_0/2$), giving rise to a frequency shift

of [46]

$$\Delta\omega^{(2)}(T) = D[1 + n(\omega_1) + n(\omega_2)], \quad (5)$$

where $n(\omega) = (e^{\hbar\omega/k_B T} - 1)^{-1}$ is the Bose-Einstein distribution of the phonon, D is a fitting parameter, and k_B is the Boltzmann constant. In the three-phonon process, phonon decay rate τ_{op}^{-1} varies with T [46] in the following way:

$$\tau_{\text{op}}^{-1}(T) = G[1 + n(\omega_1) + n(\omega_2)], \quad (6)$$

where G is a fitting parameter and $\omega_1 = \omega_2$.

The fittings to $\omega(T)$ and $\tau_{\text{op}}^{-1}(T)$ measurements with the 1.574-eV pump photon energy are presented in Fig. 10(d). $\omega(T)$ can be well described with Eqs. (3) to (5), we obtain $\omega_0 = (23.89 \pm 0.02) \times 10^{12}$ rad/s, and $\omega_1 = \omega_2 = (11.94 \pm 0.01) \times 10^{12}$ rad/s. The thermal expansion term contributes only a small portion to the frequency shift, and the fitting is not sensitive to the exact values of the related parameters. However, the fitting to $\tau_{\text{op}}^{-1}(T)$ with Eq. (6) is less satisfactory. In addition to the anharmonic phonon-phonon interaction, there may exist other ways for annihilating the A_{1g} coherent phonons in FGT, including the reexcitation of the hot carrier by the coherent phonons, and the anti-Stokes Raman scatter-

ing, in which a photon of the probe laser absorbs a phonon and emits a blue-shifted photon.

V. CONCLUSION

Strong enhancement of the A_{1g} coherent phonon excitation in FGT is demonstrated via the femtosecond transient optical spectroscopy measurements. The A_{1g} coherent phonon excitation is strongly dependent on pump photon energy, and the maximum coherent phonon excitation occurs at 1.574 eV, as a result of the resonance Raman effect when pump photon energy is tuned to an electronic transition in FGT. The A_{1g} coherent phonon excitation in FGT follows the ISRS mechanism. There is a linear relation between A_{1g} coherent phonon excitation and pump laser fluence, and photosusceptibility of the A_{1g} coherent phonon excitation is the highest at 1.574 eV. The intense A_{1g} coherent phonon excitation also modifies the dynamics of hot carrier decay and coherent phonon decay.

ACKNOWLEDGMENT

This work was sponsored by Southwest Jiaotong University.

-
- [1] T. Kampfrath, K. Tanaka, and K. A. Nelson, *Nat. Photon.* **7**, 680 (2013).
- [2] D. Fausti, R. I. Tobey, N. Dean, S. Kaiser, A. Dienst, M. Hoffmann, S. Pyon, T. Takayama, H. Takagi, and A. Cavalleri, *Science* **331**, 189 (2011).
- [3] W. Hu, S. Kaiser, D. Nicoletti, C. R. Hunt, I. Gierz, M. C. Hoffmann, M. Le Tacon, T. Loew, B. Keimer, and A. Cavalleri, *Nat. Mater.* **13**, 705 (2014).
- [4] T. Qi, Y. H. Shin, K. L. Yeh, K. A. Nelson, and A. M. Rappe, *Phys. Rev. Lett.* **102**, 247603 (2009).
- [5] X. Li, T. Qiu, J. Zhang, E. Baldini, J. Lu, A. M. Rappe, and K. A. Nelson, *Science* **364**, 1079 (2019).
- [6] C. Vaswani, L.-L. Wang, D. H. Mudiyansele, Q. Li, P. M. Lozano, G. D. Gu, D. Cheng, B. Song, L. Luo, R. H. J. Kim, C. Huang, Z. Liu, M. Mootz, I. E. Perakis, Y. Yao, K. M. Ho, and J. Wang, *Phys. Rev. X* **10**, 021013 (2020).
- [7] X. Yang, L. Luo, C. Vaswani, X. Zhao, Y. Yao, D. Cheng, Z. Liu, R. H. Kim, X. Liu, M. Dobrowolska-Furdyna, J. K. Furdyna, I. E. Perakis, C. Wang, K. Ho, and J. Wang, *npj Quantum Mater.* **5**, 13 (2020).
- [8] A. D. Caviglia, R. Scherwitzl, P. Popovich, W. Hu, H. Bromberger, R. Singla, M. Mitrano, M. C. Hoffmann, S. Kaiser, P. Zubko, S. Gariglio, J. M. Triscone, M. Först, and A. Cavalleri, *Phys. Rev. Lett.* **108**, 136801 (2012).
- [9] M. Först, C. Manzoni, S. Kaiser, Y. Tomioka, Y. Tokura, R. Merlin, and A. Cavalleri, *Nat. Phys.* **7**, 854 (2010).
- [10] D. Mills, *Phys. Rev. B* **35**, 9278 (1987).
- [11] H. J. Zeiger, J. Vidal, T. K. Cheng, E. P. Ippen, G. Dresselhaus, and M. S. Dresselhaus, *Phys. Rev. B* **45**, 768 (1992).
- [12] A. V. Kuznetsov and C. J. Stanton, *Phys. Rev. Lett.* **73**, 3243 (1994).
- [13] G. A. Garrett, T. F. Albrecht, J. F. Whitaker, and R. Merlin, *Phys. Rev. Lett.* **77**, 3661 (1996).
- [14] R. Merlin, *Solid State Commun.* **102**, 207 (1997).
- [15] A. F. May, S. Calder, C. Cantoni, H. Cao, and M. A. McGuire, *Phys. Rev. B* **93**, 014411 (2016).
- [16] B. Chen, J. Yang, H. Wang, M. Imai, H. Ohta, C. Michioka, K. Yoshimura, and M. Fang, *J. Phys. Soc. Jpn.* **82**, 124711 (2013).
- [17] S. Liu, X. Yuan, Y. Zou, Y. Sheng, C. Huang, E. Zhang, J. Ling, Y. Liu, W. Wang, C. Zhang *et al.*, *npj 2D Mater. Appl.* **1**, 30 (2017).
- [18] J. Yi, H. Zhuang, Q. Zou, Z. Wu, G. Cao, S. Tang, S. Calder, P. Kent, D. Mandrus, and Z. Gai, *2D Mater.* **4**, 011005 (2016).
- [19] X. Wang, J. Tang, X. Xia, C. He, J. Zhang, Y. Liu, C. Wan, C. Fang, C. Guo, W. Yang, Y. Guang, X. Zhang, H. Xu, J. Wei, M. Liao, X. Lu, J. Feng, X. Li, Y. Peng, H. Wei, R. Yang, D. Shi, X. Zhang, Z. Han, Z. Zhang, G. Zhang, G. Yu, and X. Han, *Sci. Adv.* **5**, eaaw8904 (2019).
- [20] Q. Li, M. Yang, C. Gong, R. V. Chopdekar, A. T. N'Diaye, J. Turner, G. Chen, A. Scholl, P. Shafer, E. Arenholz, A. K. Schmid, S. Wang, K. Liu, N. Gao, A. S. Admasu, S.-W. Cheong, C. Hwang, J. Li, F. Wang, X. Zhang, and Z. Qiu, *Nano Lett.* **18**, 5974 (2018).
- [21] S. Albarakati, C. Tan, Z.-J. Chen, J. G. Partridge, G. Zheng, L. Farrar, E. L. Mayes, M. R. Field, C. Lee, Y. Wang, Y. Xiong, M. Tian, F. Xiang, A. R. Hamilton, O. A. Tretiakov, D. Culcer, Y.-J. Zhao, and L. Wang, *Sci. Adv.* **5**, eaaw0409 (2019).
- [22] J. Xu, W. A. Phelan, and C.-L. Chien, *Nano Lett.* **19**, 8250 (2019).
- [23] N. Li, W. Liang, and S.-N. Luo, *Phys. Rev. B* **101**, 014304 (2020).
- [24] O. V. Misochko, M. Hase, K. Ishioka, and M. Kitajima, *Phys. Rev. Lett.* **92**, 197401 (2004).
- [25] A. Q. Wu and X. Xu, *Appl. Phys. Lett.* **90**, 251111 (2007).
- [26] L. Du, J. Tang, Y. Zhao, X. Li, R. Yang, X. Hu, X. Bai, X. Wang, K. Watanabe, T. Taniguchi, D. Shi, G. Yu, X. Bai,

- T. Hasan, G. Zhang, and Z. Sun, *Adv. Funct. Mater.* **29**, 1904734 (2019).
- [27] A. Milosavljević, A. Šolajić, S. Djurdjić-Mijin, J. Pešić, B. Višić, Y. Liu, C. Petrovic, N. Lazarević, Z. V. Popović, *Phys. Rev. B* **99**, 214304 (2019).
- [28] N. Suzuki and H. Kamimura, *J. Phys. Soc. Jpn.* **35**, 985 (1973).
- [29] R. P. Prasankumar and A. J. Taylor, *Optical Techniques for Solid-State Materials Characterization* (CRC, Boca Raton, FL, 2016).
- [30] H. L. Zhuang, P. R. C. Kent, and R. G. Hennig, *Phys. Rev. B* **93**, 134407 (2016).
- [31] E. Smith and G. Dent, *Modern Raman Spectroscopy - A Practical Approach* (Wiley Online Library, 2005).
- [32] A. P. Schnyder, D. Manske, and A. Avella, *Phys. Rev. B* **84**, 214513 (2011).
- [33] T. Stevens, J. Kuhl, and R. Merlin, in *Technical Digest. Summaries of Papers Presented at the Quantum Electronics and Laser Science Conference* (IEEE, New York, 1992), pp. 164–165.
- [34] K. Sato, K. Tahara, Y. Minami, I. Katayama, M. Kitajima, H. Kawai, K. Yanagi, and J. Takeda, *Phys. Rev. B* **90**, 235435 (2014).
- [35] T. E. Stevens, J. Kuhl, and R. Merlin, *Phys. Rev. B* **65**, 144304 (2002).
- [36] V. V. Kabanov, J. Demsar, and D. Mihailovic, *Phys. Rev. Lett.* **95**, 147002 (2005).
- [37] J. J. Li, J. Chen, D. A. Reis, S. Fahy, and R. Merlin, *Phys. Rev. Lett.* **110**, 047401 (2013).
- [38] C. Gadermaier, V. Kabanov, A. Alexandrov, and D. Mihailovic, *J. Appl. Phys.* **111**, 112605 (2012).
- [39] M. A. Sentef, *Phys. Rev. B* **95**, 205111 (2017).
- [40] E. Pomarico, M. Mitrano, H. Bromberger, M. A. Sentef, A. Al-Temimy, C. Coletti, A. Stöhr, S. Link, U. Starke, C. Cacho, R. Chapman, E. Springate, A. Cavalleri, and I. Gierz, *Phys. Rev. B* **95**, 024304 (2017).
- [41] D. M. Kennes, E. Y. Wilner, D. R. Reichman, and A. J. Millis, *Nat. Phys.* **13**, 479 (2017).
- [42] J. Demsar, J. L. Sarrao, and A. J. Taylor, *J. Phys.: Condens. Matter* **18**, R281 (2006).
- [43] G. Lucazeau, *J. Raman Spectrosc.* **34**, 478 (2003).
- [44] H. Tang and I. P. Herman, *Phys. Rev. B* **43**, 2299 (1991).
- [45] M. Balkanski, R. F. Wallis, and E. Haro, *Phys. Rev. B* **28**, 1928 (1983).
- [46] P. Klemens, *Phys. Rev.* **148**, 845 (1966).